DALTON
FULL PAPER

Periodic trends in metal–metal bonding in cubane clusters, $(C_5H_5)_4M_4E_4$ [M = Cr, Mo, E = O, S]

John E. McGrady

Department of Chemistry, The University of York, Heslington, York, UK YO10 5DD.
E-mail: jem15@york.ac.uk

Received 25th January 1999, Accepted 17th March 1999

Trends in structure and bonding in a series of metal cubane clusters are examined using broken-symmetry density functional theory. For the metal–sulfur clusters, $(C_5H_5)_4Mo_4S_4$ and $(C_5H_5)_4Cr_4S_4$, the twelve cluster valence electrons are delocalised in six metal–metal single bonds, giving an approximately tetrahedral metal core. In $(C_5H_5)_4Cr_4O_4$, however, no strong Cr–Cr bonds are present, and three cluster valence electrons remain localised on each of the chromium centres. Antiferromagnetic coupling across four of the six edges of the tetrahedron, and ferromagnetic coupling across the remaining two give rise to a spin-singlet ground state and a distinct rhombic distortion. The driving force for the distortion is only 12 kJ mol^{-1}, and consequently inter- and intra-molecular steric effects may play a major role in determining the structure of the cluster in the solid state. Both chromium clusters have low-lying excited states in which the bonding pattern is completely reversed, with six Cr–Cr bonds present in $(C_5H_5)_4Cr_4O_4$ but none in $(C_5H_5)_4Cr_4S_4$. In each case the excited state lies less than 45 kJ mol^{-1} above the ground state, despite the fact that a substantial structural rearrangement is involved. Changes in metal–metal bond strength and spin polarisation energy are found to contribute approximately equally to the periodic trend towards electron localisation in the chromium clusters.

Introduction

The role of iron–sulfur clusters in biological electron transfer is well documented,[1] and as a result their physical properties have been studied using a wide variety of spectroscopic[2–4] and theoretical[5] techniques. Until very recently, all available data indicated that there was no direct metal–metal bonding present in these clusters under physiological conditions, but this view has been challenged by recent EXAFS studies on the Fe protein of the enzyme nitrogenase.[6] Reduction of the single Fe_4S_4 cluster to the all-ferrous oxidation state causes substantial structural changes, consistent with the formation of Fe–Fe bonds. This observation presents the intriguing possibility that reversible redox induced formation of metal–metal bonds may play a previously unsuspected role in the control of biological electron transfer.

A wide variety of model cubane clusters have been synthesised over the years, the most extensive series being the cyclopentadienyl-capped systems, $(C_5R_5)_4M_4E_4$ (M = Mo, Cr, Ru, Ti, V, Fe, Ir, Co; E = O, S) illustrated in Chart 1 and Table 1. Within this closely related series, the cubane unit shows a high degree of structural flexibility, from the highly distorted arrangement in $(C_5H_5)_4Ru_4S_4^{2+}$,[15] to the almost perfect tetrahedral cores found in $(C_5H_4{}^iPr)_4Mo_4S_4$ and $(C_5H_5)_4Cr_4S_4$.[8,12,13] On the basis of isoelectronic relationships, a tetrahedral core might also be anticipated for the chromium–oxygen clusters, $(C_5H_{5-x}Me_x)_4Cr_4O_4$, $x = 0,1,5$,[9–11] but in fact, only the pentamethylated system, $(C_5Me_5)_4Cr_4O_4$, exhibits six approximately equivalent Cr–Cr distances.[11] In $(C_5H_4Me)_4Cr_4O_4$, a rhombic distortion compresses the tetrahedron along one two-fold axis,[9] giving four short and two long Cr–Cr separations, while in $(C_5H_5)_4Cr_4O_4$ an additional twist about the principal axis further reduces the symmetry, giving three distinct pairs of Cr–Cr distances.[10] The contrast between $(C_5H_{5-x}Me_x)_4Cr_4O_4$ and $(C_5H_4{}^iPr)_4Mo_4S_4$ is further illustrated by their magnetic properties: the chromium clusters are all antiferromagnetic, with substantial room temperature magnetic moments, while the molybdenum species is diamagnetic. A clue to the origin of the differences between the two classes of cluster comes from a comparison of the photoelectron spectra of $(C_5H_5)_4Cr_4O_4$ and $(C_5H_4{}^iPr)_4Mo_4S_4$.[22] The absence of resolved structure in the metal ionisation band in the former prompted the authors[22] to suggest that the metal-based electrons in the chromium system are very weakly coupled, in contrast to the strong bonding present in the molybdenum analogue. If this is indeed the case, then the comparison of the molybdenum–sulfur systems with their chromium–oxygen analogues provides an ideal opportunity to examine the factors which influence the balance between electron localisation and delocalisation in cubane clusters. As a result, it may shed light on the possible role of redox induced bond formation in the biological systems.

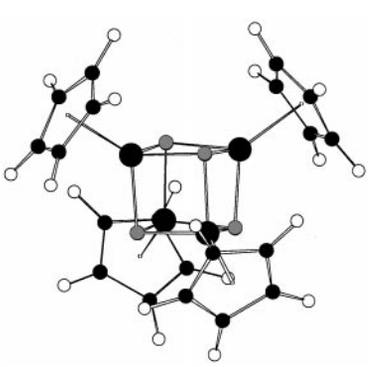

Chart 1 Structure of the $(C_5H_5)_4M_4E_4$ unit.

Several attempts to rationalise the structural properties of the metal–sulfur systems have been made using bonding models based on the interaction of four equivalent $(C_5H_5)M$ fragments.[23–26] Each fragment has three orbitals, d_{z^2}, d_{xy} and $d_{x^2-y^2}$, which are approximately non-bonding with respect to the ligands, and therefore available for metal–metal bonding. The d_{z^2} orbitals are directed radially towards the centre of the cluster, whilst d_{xy} and $d_{x^2-y^2}$ form a degenerate pair oriented tangentially around the circumference of the cluster (Fig. 1). In the limit of perfect tetrahedral symmetry [assuming effective

Table 1 Crystallographically determined structural parameters of metal–sulfur and metal–oxygen cubane clusters

Complex	Cluster valence electron count	r(M–M)/Å	r(M–E)[a]/Å	r(M–C)[a]/Å	Ref.
$(C_5Me_5)_4Ti_4S_4$	4	2 × 2.930 4 × 3.008	2.36	2.37	7
$(C_5H_4Me)_4V_4S_4^+$	7	2.852–2.855	2.28	2.25	7
$(C_5H_4Me)_4V_4S_4$	8	2.868–2.884	2.30	2.28	7
$(C_5H_4{}^iPr)_4Mo_4S_4^{2+}$	10	2 × 2.805 4 × 2.894	2.34	2.33	8
$(C_5H_4{}^iPr)_4Mo_4S_4^+$	11	2.860–2.923	2.34	2.35	8
$(C_5H_4Me)_4Cr_4O_4$	12	2 × 2.896 4 × 2.759	1.95	2.28	9
$(C_5H_5)_4Cr_4O_4$	12	2 × 2.896 2 × 2.823 2 × 2.706	1.94	2.26	10
$(C_5Me_5)_4Cr_4O_4$	12	2.828–2.840	1.95	2.27	11
$(C_5H_5)_4Cr_4S_4$	12	2.818–2.891	2.26	2.24	12
$(C_5H_4Me)_4Cr_4S_4$	12	2.822–2.848	2.25	2.24	13
$(C_5H_4{}^iPr)_4Mo_4S_4$	12	2.892–2.912	2.34	2.36	8
$(C_5H_5)_4Fe_4S_4^{2+}$	18	2 × 3.254 4 × 2.834	2.19	2.13	14
$(C_5H_4Me)_4Ru_4S_4^{2+}$	18	2.794 2 × 2.784 2 × 3.474 3.564	2.31	2.22	15
$(C_5H_5)_4Fe_4S_4^+$	19	2 × 2.652 2 × 3.188 2 × 3.319	2.21	2.11	16
$(C_5H_5)_4Fe_4S_4$	20	2 × 2.650 4 × 3.363	2.22	2.14	17
$(C_5H_4Me)_4Ru_4S_4$	20	2 × 2.753 4 × 3.601	2.33	2.22	18
$(C_5Me_5)_4Ir_4S_4^{2+}$	22	2.764 4 × 3.565 3.683	2.36	2.26	19
$(C_5H_5)_4Co_4S_4^+$	23	2 × 3.330 4 × 3.172	2.22	2.08	20
$(C_5Me_5)_4Ir_4S_4$	24	3.584–3.602	2.37	2.19	21
$(C_5H_5)_4Co_4S_4$	24	3.236–3.343	2.23	2.11	20

[a] Averaged values.

infinite rotational symmetry for the $(C_5H_5)M$ group], the four d_{z^2} orbitals transform as $a_1 + t_2$, while the eight d_{xy} and $d_{x^2-y^2}$ orbitals form a basis for $e + t_2 + t_1$ representations. Dahl and co-workers[14,23] proposed that the metal–metal bonding a_1, e and t_2 orbitals lie below their antibonding counterparts, t_1 and t_2, leading to a net order of 1.0 for each metal–metal bond in clusters such as $(C_5H_5)_4Mo_4S_4$ with twelve valence electrons. In $(C_5H_5)_4Co_4S_4$, the additional valence electrons occupy all components of the antibonding t_1 and t_2 orbitals, again giving a symmetric structure, but this time with much longer distances between the metal centres,[20] consistent with a Co–Co bond order of zero. In between these closed-shell limits, distortions from tetrahedral symmetry occur. For example, the Fe_4 cores in $(C_5H_5)_4Fe_4S_4^{2+}$ (eighteen valence electrons) and $(C_5H_5)_4Fe_4S_4$ (twenty valence electrons) are elongated and compressed respectively along one two-fold axis.[14,17] Both types of rhombic distortion can be rationalised in terms of Jahn–Teller instability arising from the partial occupancy of the degenerate t_1 and t_2 orbitals. While the Dahl bonding model has been remarkably successful in rationalising the properties of the metal–sulfur cubane clusters, the apparently anomalous properties of their chromium–oxygen analogues cannot be simply explained within the same framework. On the basis of extended Hückel calculations, Bottomley and Grein[24] proposed an alternative scheme where strong interactions with the bridging oxide ligands destabilise the metal–metal bonding a_1 orbital. The resulting ground-state configuration, $e^4t_2{}^6t_1{}^2$, would then be Jahn–Teller unstable, giving rise to a distortion from tetrahedral symmetry. More recent calculations, however, suggest that their result was an artifact of the chosen parameter set, and favour the original orbital ordering shown in Fig. 1.[10c,26] The distorted structures and non-zero room temperature magnetic moments of the chromium–oxygen clusters could also, in principle, arise from a dynamic Jahn–Teller distortion due to the thermal population of the antibonding t_1 and t_2 orbitals. This is, however, inconsistent with variable temperature crystallographic studies, which show a marginal increase, rather than decrease, in the magnitude of the rhombic distortion as the temperature is reduced.[10c] In summary, simple molecular orbital arguments based on the interactions of four equivalent $(C_5H_5)M$ units have so far failed to provide a convincing rationale for the distortions observed in $(C_5H_5)_4Cr_4O_4$.

Green and co-workers[22] noted that if the electrons in $(C_5H_5)_4Cr_4O_4$ are weakly coupled, single configuration molecular orbital methods such as those used by Dahl, Bottomley and others[23–26] are likely to be inadequate, because the effects of electron correlation are neglected. In a series of recent papers reporting density functional studies on bimetallic clusters,[27] it has been shown that this can result in the underestimation of metal–metal bond lengths by as much as 1.0 Å. The effects of electron correlation can, however, be modelled within spin-unrestricted density functional theory by removing all symmetry elements connecting the metal ions (broken-symmetry density functional theory, see methodology section), thereby permitting the electrons to localise. The result is a much improved description of antiferromagnetic coupling, and optimised metal–metal bond lengths in excellent agreement with experiment. Noodleman and Norman have shown that this broken-symmetry methodology[28] is essential for an accurate description of metal–metal interactions in tetrametallic clusters such as $Fe_4S_4(SR)_4$,[5a–c] as well as numerous other polymetallic systems.[29] A key feature of the broken-symmetry technique is

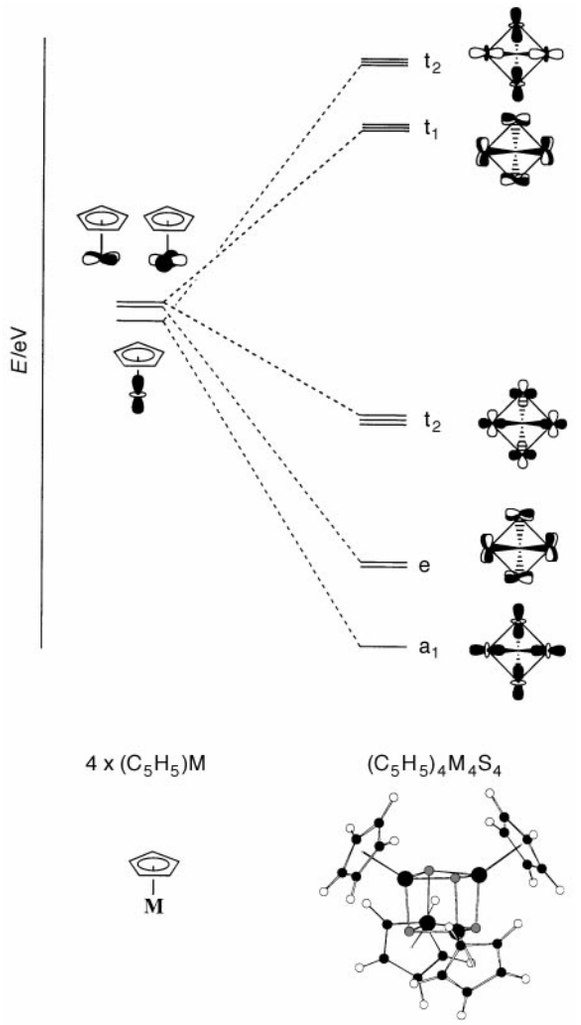

Fig. 1 Schematic molecular orbital diagram for cubanes (after refs. 23 and 26).

that it permits, but does not force, the electrons to localise. Thus, the fully delocalised electron spin density distribution characteristic of strong metal–metal bonding can be recovered if it represents a more stable situation than the localised alternative.

The broken-symmetry technique is therefore capable of modelling both weakly coupled and strongly bonded limits without bias, and is ideal for a study of periodic trends. In this paper, broken-symmetry density functional theory is used to investigate periodic trends in the structure and bonding of $(C_5H_5)_4M_4E_4$, M = Cr, Mo, E = O, S. In particular, the aim is to establish whether there is an abrupt change in electronic structure between the chromium–oxygen clusters and their molybdenum–sulfur counterparts, and whether this gives rise to the unusual structural properties of the former. The long term goal is to establish a theoretical technique capable of analysing redox-induced metal–metal bond formation in the iron–sulfur and iron–molybdenum–sulfur clusters, and the potential implications of such processes for electron transfer pathways in redox enzymes.

Methodology

All calculations described in this paper are based on approximate density functional theory, which has been used to probe structural, energetic and mechanistic problems in numerous transition metal-based systems.[30] Calculations were performed using the Amsterdam Density Functional (ADF) program Version 2.3, developed by Baerends and co-workers.[31] A double-ζ Slater-type basis set, extended with a single polarisation function, was used to describe the hydrogen, carbon, oxygen and sulfur atoms, while molybdenum and chromium were modelled with a triple-ζ basis set. Electrons in orbitals up to and including 1s {C,O}, 2p {S}, 3p {Cr} and 4p {Mo} were considered part of the core and treated in accordance with the frozen core approximation. The local density approximation was employed in all cases,[32] along with the local exchange-correlation potential of Vosko, Wilk and Nusair[33] and gradient corrections to exchange and correlation proposed by Perdew and Wang.[34] All structures were optimised using the gradient algorithm of Versluis and Ziegler.[35] The cyclopentadienyl rings were constrained to local D_{5h} symmetry, and were aligned with one carbon atom of each ring eclipsing an edge of the M_4 tetrahedron, giving a nuclear framework with D_{2d} symmetry (see Chart 1).

All four clusters in the current study have spin-singlet ground states, a situation that can be achieved in one of two ways depending on the distribution of spin density throughout the cluster. In the limit of full electron delocalisation, each of the twelve metal-based electrons, six with spin-α, six with spin-β, have equal amplitude on all four metal centres, and the electron spin density has the full symmetry of the nuclear framework [D_{2d}, Scheme 1, structure (a)]. At the opposite extreme of complete electron localisation, the spin-α electrons are concentrated on the upper half of the cluster, the spin-β electrons on the lower half, resulting in an electron spin density distribution of lower symmetry than the nuclear framework [C_{2v}, Scheme 1, structure (b)]. This localised limit can be modelled by removing all symmetry elements connecting the two halves of the cluster, and imposing an initial excess of spin-α and spin-β electron density on the upper and lower M_2 units respectively. To aid comparison between the localised and delocalised limits, orbitals will be labelled according to the representations of the C_{2v} subgroup throughout this manuscript.

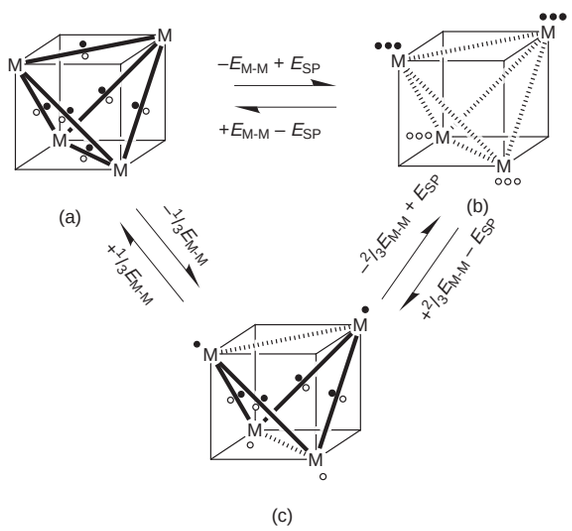

Scheme 1 Electron spin density distributions in M_4E_4 cubanes. Bold lines indicate strong metal–metal bonds, broken lines indicate weak magnetic coupling.

Results

Ground-state electronic structure of $(C_5H_5)_4Cr_4O_4$

Optimised structural parameters for the ground states of all four clusters are summarised in Table 2, along with total energies and the net spin densities per metal centre. The calculated parameters for $(C_5H_5)_4Cr_4O_4$ are in excellent accord with crystallographic data, with Cr–Cr, Cr–O and Cr–C separations lying within 0.06 Å of the experimentally determined values. Most significantly, a distinct ground-state

Table 2 Optimised energies, spin distributions and structural parameters for ground and excited states of $(C_5H_5)_4M_4E_4$ (M = Cr, Mo, E = O, S)

		Configuration, $\Gamma^{\alpha,\beta}$	r(M–M)/Å	r(M–E)/Å	r(M–C)/Å	Relative energy/kJ mol^{-1}	Net spin
Ground-state	$(C_5H_5)_4Cr_4O_4$	$a_1^{2,2}a_2^{1,1}b_1^{2,1}b_2^{1,2}$	2 × 2.886 4 × 2.753	1.950	2.306	0.00	±2.78
	$(C_5H_5)_4Cr_4S_4$	$a_1^{3,3}a_2^{1,1}b_1^{1,1}b_2^{1,1}$	2 × 2.800 4 × 2.802	2.250	2.253	0.00	0.00
	$(C_5H_5)_4Mo_4O_4$	$a_1^{3,3}a_2^{1,1}b_1^{1,1}b_2^{1,1}$	2 × 2.674 4 × 2.682	2.088	2.454	0.00	0.00
	$(C_5H_5)_4Mo_4S_4$	$a_1^{3,3}a_2^{1,1}b_1^{1,1}b_2^{1,1}$	2 × 2.930 4 × 2.950	2.402	2.411	0.00	0.00
Excited-state	$(C_5H_5)_4Cr_4O_4$	$a_1^{3,3}a_2^{1,1}b_1^{1,1}b_2^{1,1}$	2 × 2.466 4 × 2.471	1.919	2.276	+46	0.00
	$(C_5H_5)_4Cr_4S_4$	$a_1^{2,2}a_2^{1,1}b_1^{2,1}b_2^{1,2}$	2 × 3.250 4 × 2.973	2.326	2.278	+43	±2.53
	$(C_5H_5)_4Mo_4O_4$	$a_1^{2,2}a_2^{1,1}b_1^{2,1}b_2^{1,2}$	2 × 3.068 4 × 2.605	2.096	2.456	+110	±0.76
	$(C_5H_5)_4Mo_4S_4$	$a_1^{2,2}a_2^{1,1}b_1^{2,1}b_2^{1,2}$	2 × 3.358 4 × 2.870	2.436	2.407	+215	±0.76

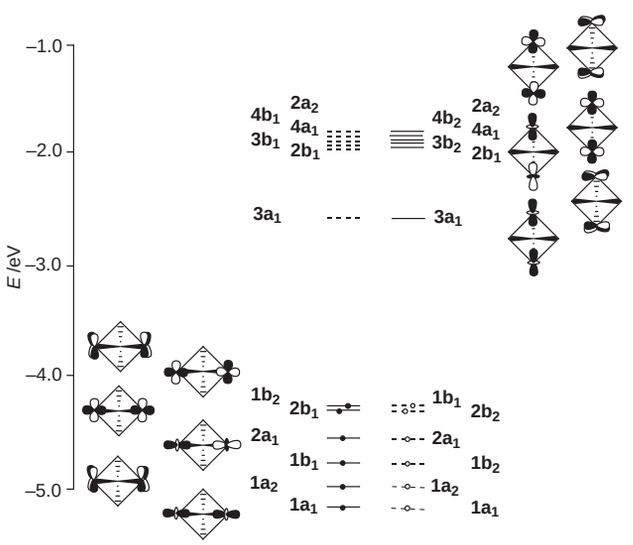

Fig. 2 Molecular orbital diagram for the broken-symmetry ground state of $(C_5H_5)_4Cr_4O_4$: spin-α orbitals are shown as full lines, spin-β orbitals as dashed lines. Orbitals which are predominantly involved in metal–ligand, rather than metal–metal, interactions are not shown. Sketches are shown only for the spin-α orbitals, their spin-β counterparts are identical, but localised on the opposite half of the cluster.

rhombic distortion emerges, with two long and four short Cr–Cr distances. The net spin densities of ±2.78 per metal centre indicate that the electrons are localized, with a spin density distribution similar to that shown in Scheme 1, structure (b). The most logical starting point for the discussion of the molecular orbital structure is therefore not the delocalised view implicit in the Dahl model, but rather that of four isolated d^3 single ions in their spin-quartet ground states. The molecular orbital diagram for the broken-symmetry ground state of $(C_5H_5)Cr_4O_4$ is summarised in Fig. 2, with orbitals localised on the upper and lower halves of the cluster shown on the left and right sides respectively. On the upper half, the in-phase and out-of-phase combinations of the radially oriented d_{z^2} orbitals transform as $a_1 + b_1$, while their tangential counterparts, d_{xy} and $d_{x^2-y^2}$, transform as $a_1 + b_1$ and $a_2 + b_2$ respectively, giving a total of $2a_1 + a_2 + 2b_1 + b_2$ symmetry orbitals. The orbitals on the lower half transform in a similar manner, except that the rotation by 90° about the principal axis interconverts the b_1 and b_2 symmetry labels, yielding $2a_1 + a_2 + b_1 + 2b_2$ symmetry orbitals. Where metal–metal interactions are weak, each of these twelve symmetry orbitals remains singly occupied, those on the upper half of the cluster by spin-α electrons, those on the lower half by spin-β, leading to a ground-state electronic configuration $\Gamma^{\alpha,\beta} = a_1^{2,2}a_2^{1,1}b_1^{2,1}b_2^{1,2}$. In terms of magnetic coupling, the chromium centres within each dimeric unit are ferromagnetically coupled (spins parallel), while the two dimeric units are coupled antiferromagnetically (spins antiparallel).

The extent of the rhombic distortion described in the introduction is defined by the angle θ between the centroid and two chromium centres in either the upper or lower half of the cluster. Where $\theta = 109.5°$, the M_4 core is perfectly tetrahedral, while larger values correspond to an increased separation between the ferromagnetically coupled chromium centres. The dependence on θ of the energies of the occupied spin-α orbitals of $(C_5H_5)_4Cr_4O_4$ is summarised in Fig. 3 (the corresponding spin-β orbitals, localised on the opposite half of the cluster, behave in identical fashion). As θ increases, the major effect is a stabilisation of the $2b_1$ orbital, an antibonding combination of the $d_{x^2-y^2}$ orbitals on the two centres. Thus, it is the reduction in antibonding character between the two ferromagnetically coupled chromium centres that provides the driving force for the rhombic distortion in $(C_5H_5)_4Cr_4O_4$. The poor overlap between the small chromium 3d orbitals makes this driving force relatively weak, and the optimised structure ($\theta = 114.7°$) is only 12 kJ mol^{-1} more stable than the perfectly tetrahedral one ($\theta = 109.5°$).

The calculations described so far do not address the question of the origin of the twist observed in the crystal structure of $(C_5H_5)_4Cr_4O_4$, because this type of distortion does not lie on the C_{2v}-symmetric potential energy surface. The structure was therefore re-optimised using C_2 point symmetry, with one Cr_2 unit twisted relative to the other. The potential energy curve describing the twist is found to be extremely flat (<10 kJ mol^{-1} above the minimum for rotations of up to 10° about the principal axis), but no evidence was found for additional minima, optimisation always resulting in a C_{2v}-symmetric structure. In conclusion, the electronically-favoured structure for the $(C_5H_5)_4Cr_4O_4$ system is the rhombically distorted one, with both the tetrahedral and twisted structures lying approximately 10–12 kJ mol^{-1} higher in energy. The almost perfectly tetrahedral structure observed for pentamethylated species, $(C_5Me_5)_4Cr_4O_4$, along with the low-symmetry distortion seen in $(C_5H_5)_4Cr_4O_4$, must therefore arise because the weak electronic driving force favouring the distortion is of similar magnitude to intra- or inter-molecular steric interactions.

Ground-state electronic structure of $(C_5H_5)_4Cr_4S_4$, $(C_5H_5)_4Mo_4O_4$ and $(C_5H_5)_4Mo_4S_4$

In the metal–sulfur clusters, the optimised ground-state structural parameters are again in excellent agreement with crystallographic data. In particular, no rhombic distortion is

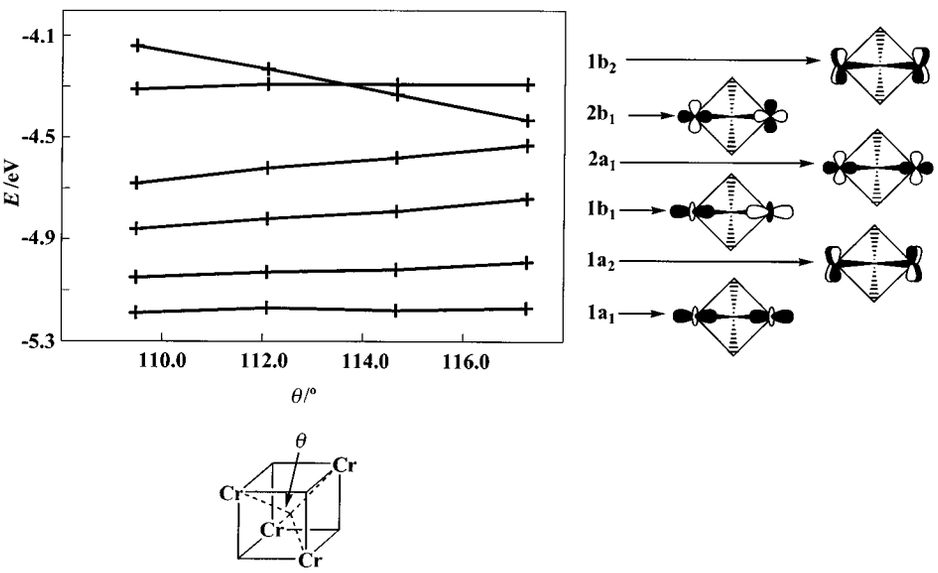

Fig. 3 Walsh diagram showing the dependence on θ of the energy of the occupied orbitals of $(C_5H_5)_4Cr_4O_4$.

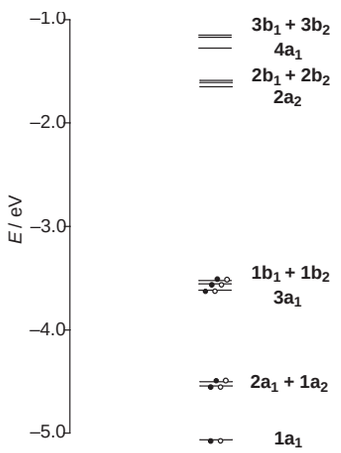

Fig. 4 Molecular orbital diagram for the ground state of $(C_5H_5)_4Mo_4S_4$: no distinction is made on the basis of either spin or spatial distribution, as all cluster valence electrons are delocalised. Orbitals which are predominantly involved in metal–ligand, rather than metal–metal, interactions are not shown.

Table 3 Descent in symmetry from T_d to C_{2v}

T_d	C_{2v}
a_1	a_1
e	$a_1 + a_2$
t_1	$a_2 + b_1 + b_2$
t_2	$a_1 + b_1 + b_2$

predicted, consistent with the presence of six equivalent metal–metal single bonds lying along each of the edges of the tetrahedron. A molecular orbital diagram for the ground state of $(C_5H_5)_4Mo_4S_4$ is illustrated in Fig. 4 [the qualitative features of the molecular orbital diagrams for $(C_5H_5)_4Cr_4S_4$ and $(C_5H_5)_4Mo_4O_4$ are identical]. In contrast to Fig. 2, no distinction is made on the basis of either spin or spatial distribution, because the net spin densities of zero indicate that all metal-based electrons are fully delocalised over the whole cluster [Scheme 1, structure (a)]. The occupied manifold contains three narrow bands, made up, in ascending order, of $1a_1$, $2a_1 + 1a_2$ and $3a_1 + 1b_1 + 1b_2$, giving a ground-state electronic configuration of $\Gamma^{\alpha,\beta} = a_1^{3,3}a_2^{1,1}b_1^{1,1}b_2^{1,1}$, which correlates directly with the $\Gamma = a_1^2e^4t_2^6$ configuration shown in Fig. 1 (see Table 3). Thus, when the electrons are delocalised over the whole cluster, the bonding model obtained from the broken-symmetry technique converges with that proposed by Dahl and others.[14,23] In contrast, the $\Gamma^{\alpha,\beta} = a_1^{2,2}a_2^{1,1}b_1^{2,1}b_2^{1,2}$ ground-state configuration of the chromium–oxygen analogue correlates with an excited state, $\Gamma = a_1^2e^4t_2^4t_1^2$, in tetrahedral symmetry, confirming that the Dahl model is inappropriate in the limit of weak metal–metal bonding.

Excited-state properties

Despite the fact that the electron spin-density distributions are very different for $(C_5H_5)_4Cr_4O_4$ and $(C_5H_5)_4Cr_4S_4$, their ground-state configurations differ only in the location of two electrons, which are either in $2b_1\alpha/2b_2\beta$ (localised) or $3a_1\alpha/\beta$ (delocalised). Thus population of a doubly excited state may cause substantial changes in the electron distribution, and hence in the structure of the cluster. In $(C_5H_5)_4Cr_4O_4$, promotion of two electrons from $2b_1\alpha/2b_2\beta$ to $3a_1\alpha/\beta$ causes the metal-based electrons to delocalise completely, resulting in a net spin density of zero. The Cr–Cr distances contract by 0.3–0.4 Å, consistent with the formation of six Cr–Cr single bonds, and the rhombic distortion disappears. In contrast, precisely the opposite is observed in the excited state of $(C_5H_5)_4Cr_4S_4$ ($\Gamma^{\alpha,\beta} = a_1^{2,2}a_2^{1,1}b_1^{2,1}b_2^{1,2}$), where the metal-based electrons localise (net spin densities = ±2.53), the Cr–Cr separations lengthen by 0.35–0.45 Å, and a strong rhombic distortion emerges. Perhaps the most surprising aspect of this observation is that in each case the excited state lies less than 45 kJ mol^{-1} above the ground state, indicating that gross structural rearrangements, involving changes of almost 0.5 Å in metal–metal bond lengths, can be energetically facile. Moreover, not only do the two clusters lie close to the localised/delocalised borderline, they are also symmetrically placed on either side of it. Accordingly, the structure of the mixed oxide–sulfide cluster, $(C_5H_5)_4Cr_4S_2O_2$ has been optimised in both electronic configurations, and the localised and delocalised states are found to be separated by only 2 kJ mol^{-1}, despite having Cr–Cr separations which differ by over 0.3 Å. This observation suggests that, given a judicious choice of ligands, dramatic changes in cluster structure and bonding might be induced by very minor electronic or steric perturbations.

Despite the very similar ground-state properties of $(C_5H_5)_4Cr_4S_4$, $(C_5H_5)_4Mo_4O_4$ and $(C_5H_5)_4Mo_4S_4$, the excited-state properties of the two molybdenum clusters differ significantly from those of the chromium–sulfur system described above. In both molybdenum clusters, two of the six Mo–Mo separations increase by approximately 0.4 Å, while the remaining

four contract slightly, giving a very strong rhombic distortion [Scheme 1, structure (c)]. The net spin densities of +0.76 confirm that only two of the six Mo–Mo bonds have been broken, which is precisely the result that might have been anticipated on the basis of the bonding/antibonding character of the $2b_1/2b_2$ and $3a_1$ orbitals. The former are antibonding with respect to the metal–metal bonds, while the latter are bonding (see Fig. 2), and so the total bond order for the clusters is reduced from six to four in the excited state. This then raises the question of why promotion of the same two electrons in $(C_5H_5)_4Cr_4S_4$ causes the cleavage of all six, rather than just two, of the metal–metal bonds. In the following section, the different properties of the chromium and molybdenum systems are rationalised in terms of the competing effects of metal–metal bond strength and spin polarisation energy.

The balance between localised and delocalised electron distributions

In previous papers[27] it has been established that the relative stability of localised and delocalised electron density distributions is determined by the balance between the strength of the metal–metal bonds, favouring delocalisation, and the spin polarisation energy, favouring localisation. The absolute magnitude of this spin polarisation energy is related to $n[n-1]/2$, where n is the number of unpaired electrons per metal centre. A quantitative estimate of the magnitude of these two competing terms can be obtained by defining a reference configuration in which neither metal–metal bonding nor spin polarisation are present. In this case, the appropriate configuration is spin restricted $\Gamma = 1a_1^{\,1}2a_1^{\,1}1a_2^{\,1}3a_1^{\,1}1b_1^{\,1}1b_2^{\,1}2a_2^{\,1}2b_1^{\,1}2b_2^{\,1}4a_1^{\,1}3b_1^{\,1}3b_2^{\,1}$ (see Fig. 4), where single occupation of all bonding and antibonding combinations ensures a net metal–metal bond order of zero. The metal–metal bond energy (denoted E_{M-M}) is then taken as the difference in energy between the reference configuration and that where all electrons are involved in metal–metal bonds ($\Gamma^{\alpha,\beta} = a_1^{\,3,3}a_2^{\,1,1}b_1^{\,1,1}b_2^{\,1,1}$). Similarly, the spin polarisation energy, E_{SP}, is taken as the difference between the reference configuration and one in which there are three unpaired electrons per metal centre. Unfortunately the energy of the $\Gamma^{\alpha,\beta} = a_1^{\,2,2}a_2^{\,1,1}b_1^{\,2,1}b_2^{\,1,2}$ broken-symmetry state described in the previous section is not appropriate, because in the molybdenum clusters, the electrons are only partially localised. Instead, a high-spin configuration, $\Gamma^{\alpha,\beta} = a_1^{\,4,0}a_2^{\,2,0}b_1^{\,3,0}b_2^{\,3,0}$, with twelve unpaired electrons, is defined corresponding to single occupation of all metal-based bonding and antibonding orbitals. In this configuration, which differs from the localised broken-symmetry state only in the orientations of the spins on the two halves of the molecule, maximum spin polarisation is assured, while metal–metal bonding is completely eliminated. A detailed discussion of this form of analysis is given in ref. 27(*c*).

Values of E_{M-M} and E_{SP} for the four clusters are summarised in Table 4. The spin polarisation energy falls by over 260 kJ mol^{-1} on replacement of chromium by molybdenum because the more diffuse 4d orbitals increase the average separation between the electrons. Replacement of oxygen with sulfur has a similar, although smaller, effect due to the greater covalence of the metal–sulfur bond, which also increases the average interelectronic separation. Trends in E_{M-M} are exactly opposite to those in E_{SP}, because strong metal–metal bonds are favoured by strong orbital overlap, and therefore by large metal d orbitals. Thus E_{M-M} increases when chromium is replaced by molybdenum, and when oxygen is replaced by sulfur. In both molybdenum systems, $E_{M-M} \gg E_{SP}$, indicating that the strength of six metal–metal bonds outweighs the spin polarisation, and so the delocalised electron spin density distribution prevails. For the corresponding chromium clusters, the increase in E_{SP} and concomitant decrease in E_{M-M} combine to cause a shift towards the localised limit. The greater tendency of heavier members of the triad to form metal–metal bonds is well established, and is usually interpreted solely in terms of the more effective overlap afforded by the larger 4d and 5d orbitals. The analysis presented here shows that changes in orbital overlap are only one factor, and in fact for the oxide clusters, the decrease in spin polarisation energy is more important. Thus when considering the tendency of a given complex to form metal–metal bonds, it is important to consider not only the potential gain in energy associated with orbital overlap, but also the loss of spin polarisation energy associated with the delocalisation of the electrons. For $(C_5H_5)_4Cr_4S_4$, E_{M-M} remains significantly larger than E_{SP}, and accordingly the electrons remain delocalised, but for $(C_5H_5)_4Cr_4O_4$, the two terms are almost identical. The additional stability associated with the antiferromagnetic coupling in the broken-symmetry state (rather than ferromagnetic in the high-spin state on which this analysis is based) is then sufficient to tip the balance in favour of localisation.

Table 4 Metal–metal bond (E_{M-M}) and spin polarisation (E_{SP}) energies

	E_{M-M}/kJ mol^{-1}	E_{SP}/kJ mol^{-1}
$(C_5H_5)_4Cr_4O_4$	798	788
$(C_5H_5)_4Cr_4S_4$	915	767
$(C_5H_5)_4Mo_4O_4$	992	514
$(C_5H_5)_4Mo_4S_4$	1222	502

The different structural changes associated with the promotion of two electrons in the molybdenum and chromium clusters can also be rationalised in terms of the balance between spin polarisation energy and metal–metal bond strength. As noted in the previous section, the bonding/antibonding properties of the orbitals would suggest that only two of the six bonds should be affected in the excited state, changing the total energy associated with the metal–metal bonds from E_{M-M} to approximately $2/3E_{M-M}$ [Scheme 1, structures (a)–(c)]. If polarisation of the core- and ligand-based electrons is neglected, there is no increase in spin polarisation energy associated with this transition, because only a single unpaired electron is generated per metal centre ($n[n-1]/2 = 0$). Cleavage of the remaining four bonds completely eliminates the residual metal–metal bonding ($2/3E_{M-M}$), but this is now offset by the emergence of the spin polarisation energy, E_{SP}, associated with the generation of three unpaired electrons per metal centre [Scheme 1, structures (a)–(c)]. The balance between partial and complete bond cleavage in the excited state is therefore determined by the relative magnitudes of $2/3E_{M-M}$ (favouring retention of four bonds) and E_{SP} (favouring complete cleavage). For the molybdenum clusters, $2/3E_{M-M} \gg E_{SP}$, and the metal–metal bonds are therefore strong enough to resist complete electron localisation. In contrast, $E_{SP} > 2/3E_{M-M}$ for $(C_5H_5)_4Cr_4S_4$, and the large gain in spin polarisation energy outweighs the combined strength of the four residual Cr–Cr bonds, causing complete electron localisation.

Conclusions

In this paper, the delicate balance between strong metal–metal bonding and weak antiferromagnetic coupling in metal cubane clusters has been illustrated. Only relatively minor structural and electronic changes are necessary to cause an abrupt transition from one regime to the other. The degree of electron localisation is determined by the competition between orbital overlap (favouring delocalisation) and spin polarisation energy (favouring localisation). For the molybdenum clusters, metal–metal bonding is strong, and the electrons are delocalised in the ground state, giving an almost perfectly tetrahedral M_4 core. For the chromium systems, the two terms are more delicately balanced, and in $(C_5H_5)_4Cr_4O_4$, the spin polarisation term dominates, causing the electrons to localise. In this case, the metal-based electrons are antiferromagnetically coupled across four

edges of the tetrahedron, and ferromagnetically coupled across the other two, giving rise to a rhombic distortion. Both chromium clusters have low-lying excited states (<45 kJ mol^{-1} above the ground state) in which the nature of the metal–metal bonding is completely reversed relative to the ground state (weak coupling for the sulfur system, strong bonding for the oxygen analogue). The transition from ground to excited state is therefore associated with major structural rearrangements, despite the relatively low energy involved. In future work, the influence of redox changes on metal–metal bonding in related clusters will be analysed, with the aim of determining whether electron transfer at biologically attainable potentials can also induce abrupt transitions from one bonding regime to another.

References

1 R. Cammack, *Adv. Inorg. Chem.*, 1992, **38**, 281; H. Beinert, R. H. Holm and E. Münck, *Science*, 1997, **277**, 653.
2 W. R. Hagen, *Adv. Inorg. Chem.*, 1992, **38**, 165; I. Bertini, S. Ciurli and C. Luchinat, *Struct. Bonding* (*Berlin*), 1995, **83**, 1.
3 S. J. Yoo, Z. Hu, C. Goh, E. L. Bominaar, R. H. Holm and E. Münck, *J. Am. Chem. Soc.*, 1997, **119**, 8732; E. P. Day, J. Peterson, J. J. Bonvoisin, I. Moura and J. J. G. Moura, *J. Biol. Chem.*, 1988, **263**, 3684.
4 H. C. Angove, S. J. Yoo, B. K. Burgess and E. Münck, *J. Am. Chem. Soc.*, 1997, **119**, 8730; P. A. Lindahl, E. P. Day, T. A. Kent, W. H. Orme-Johnson and E. Münck, *J. Biol. Chem.*, 185, **260**, 11160.
5 (*a*) L. Noodleman and D. A. Case, *Adv. Inorg. Chem.*, 1992, **38**, 423; (*b*) A. Aizman and D. A. Case, *J. Am. Chem. Soc.*, 1982, **104**, 3269; (*c*) L. Noodleman, C. Y. Peng, D. A. Case and J.-M. Mouesca, *Coord. Chem. Rev.*, 1995, **144**, 199; (*d*) A. J. Thomson, *J. Chem. Soc., Dalton Trans.*, 1981, 1180; (*e*) A. Ceulemans and P. W. Fowler, *Inorg. Chim. Acta*, 1985, **105**, 75.
6 K. B. Musgrave, H. C. Angove, B. K. Burgess, B. Hedman and K. O. Hodgson, *J. Am. Chem. Soc.*, 1998, **120**, 5325.
7 J. Darkwa, J. R. Lockemeyer, P. D. W. Boyd, T. B. Rauchfuss and A. L. Rheingold, *J. Am. Chem. Soc.*, 1988, **110**, 141.
8 J. A. Bandy, C. E. Davies, J. C. Green, M. L. H. Green, K. Prout and D. P. S. Rodgers, *J. Chem. Soc., Chem. Commun.*, 1983, 1395.
9 I. L. Eremenko, S. E. Nefedov, A. A. Pasynskii, B. Orazsakhatov, O. G. Ellert, Yu. T. Struchkov, A. I. Yanovsky and D. V. Zagorevsky, *J. Organomet. Chem.*, 1989, **368**, 185.
10 (*a*) F. Bottomley, D. E. Paez and P. S. White, *J. Am. Chem. Soc.*, 1981, **103**, 5581; (*b*) F. Bottomley, D. E. Paez and P. S. White, *J. Am. Chem. Soc.*, 1982, **104**, 5651; (*c*) F. Bottomley, D. E. Paez, L. Sutin, P. S. White, F. H. Köhler, R. C. Thompson and N. P. C. Westwood, *Organometallics*, 1990, **9**, 2443.
11 F. Bottomley, J. Chen, S. M. MacIntosh and R. C. Thompson, *Organometallics*, 1991, **10**, 906.
12 C. Wei, L.-Y. Goh, R. F. Bryan and E. Sinn, *Acta Crystallogr., Sect. C*, 1986, **42**, 796.
13 A. A. Pasynskii, I. L. Eremenko, Yu. V. Rakitin, V. M. Novotortsev, O. G. Ellert, V. T. Kalinnikov, V. E. Shklover, Yu. T. Struchkov, S. V. Lindeman, T. Kh. Kurbanov and G. Sh. Gasanov, *J. Organomet. Chem.*, 1983, **248**, 309.
14 Trinh-Toan, B. K. Teo, J. A. Ferguson, T. J. Meyer and L. F. Dahl, *J. Am. Chem. Soc.*, 1977, **99**, 408.
15 E. J. Houser, J. Amarasekera, T. B. Rauchfuss and S. R. Wilson, *J. Am. Chem. Soc.*, 1991, **113**, 7440; E. J. Houser, T. B. Rauchfuss and S. R. Wilson, *Inorg. Chem.*, 1993, **32**, 4069.
16 Trinh-Toan, W. P. Fehlhammer and L. F. Dahl, *J. Am. Chem. Soc.*, 1977, **99**, 402.
17 R. A. Schunn, C. J. Fritchie and C. T. Prewitt, *Inorg. Chem.*, 1966, **5**, 892; C. H. Wei, G. R. Wilkes, P. M. Treichel and L. F. Dahl, *Inorg. Chem.*, 1966, **5**, 900.
18 J. Amarasekera, T. B. Rauchfuss and S. R. Wilson, *J. Chem. Soc., Chem. Commun.*, 1989, 14.
19 A. Venturelli and T. B. Rauchfuss, *J. Am. Chem. Soc.*, 1994, **116**, 4824.
20 G. L. Simon and L. F. Dahl, *J. Am. Chem. Soc.*, 1973, **95**, 2164.
21 D. A. Dobbs and R. G. Bergman, *J. Am. Chem. Soc.*, 1992, **114**, 6908.
22 C. E. Davies, J. C. Green, N. Kaltsoyannis, M. A. MacDonald, J. Qin, T. B. Rauchfuss, C. M. Redfern, G. H. Stringer and M. G. Woolhouse, *Inorg. Chem.*, 1992, **31**, 3779.
23 A. S. Faust and L. F. Dahl, *J. Am. Chem. Soc.*, 1970, **92**, 7337; G. L. Simon and L. F. Dahl, *J. Am. Chem. Soc.*, 1973, **95**, 2175.
24 F. Bottomley and F. Grein, *Inorg. Chem.*, 1982, **21**, 4170.
25 S. Harris, *Inorg. Chem.*, 1987, **26**, 4278; S. Harris, *Polyhedron*, 1989, **8**, 2843; C. S. Bahn, A. Tan and S. Harris, *Inorg. Chem.*, 1998, **37**, 2770.
26 P. D. Williams and M. D. Curtis, *Inorg. Chem.*, 1986, **25**, 4562.
27 (*a*) J. E. McGrady, R. Stranger and T. Lovell, *Inorg. Chem.*, 1998, **37**, 3802; (*b*) J. E. McGrady, R. Stranger and T. Lovell, *J. Phys. Chem. A*, 1997, **101**, 6265; (*c*) J. E. McGrady, T. Lovell and R. Stranger, *Inorg. Chem.*, 1997, **36**, 3242; (*d*) T. Lovell, J. E. McGrady, R. Stranger and S. A. Macgregor, *Inorg. Chem.*, 1996, **35**, 3079; (*e*) J. E. McGrady and R. Stranger, *J. Am. Chem. Soc.*, 1997, **119**, 8512.
28 L. Noodleman and J. G. Norman, Jr., *J. Chem. Phys.*, 1979, **70**, 4903; L. Noodleman, *J. Chem. Phys.*, 1981, **74**, 5737.
29 C. A. Brown, G. J. Remar, R. L. Musselman and E. I. Solomon, *Inorg. Chem.*, 1995, **34**, 688; P. K. Ross and E. I. Solomon, *J. Am. Chem. Soc.*, 1991, **113**, 3246; H. Jacobsen, H.-B. Kraatz, T. Ziegler and P. M. Boorman, *J. Am. Chem. Soc.*, 1992, **114**, 7851; A. Bencini and D. Gatteschi, *J. Am. Chem. Soc.*, 1986, **108**, 5763; J. Andzelm and E. Wimmer, *J. Chem. Phys.*, 1992, **96**, 1280; K. E. Edgecombe and A. D. Becke, *Chem. Phys. Lett.*, 1995, **244**, 427; N. A. Baykara, B. N. McMaster and D. R. Salahub, *Mol. Phys.*, 1984, **52**, 891.
30 T. Ziegler, *Chem. Rev.*, 1991, **91**, 651.
31 ADF 2.3.0, Theoretical Chemistry, Vrije Univeriteit, Amsterdam, E. J. Baerends, D. E. Ellis and P. Ros, *Chem. Phys.*, 1973, **2**, 42; G. te Velde and E. J. Baerends, *J. Comput. Phys.*, 1992, **99**, 84.
32 R. G. Parr and W. Yang, *Density Functional Theory of Atoms and Molecules*, Oxford University Press, New York, 1989.
33 S. H. Vosko, L. Wilk and M. Nusair, *Can. J. Phys.*, 1980, **58**, 1200.
34 J. P. Perdew and Y. Wang, *Phys. Rev. B*, 1991, **44**, 13298; J. P. Perdew and Y. Wang, *Phys. Rev. B*, 1992, **45**, 13244.
35 L. Versluis and T. Ziegler, *J. Chem. Phys.*, 1988, **88**, 322.

Paper 9/00660E